Chemistry of C_2S and C_3S in L1544 with NSRT

Rong Ma[1,2], Xiaohu Li[1,3,4*], Donghui Quan[5,1*], Juan Tuo[1,3], Ryszard Szczerba[1,3], Jarken Esimbek[1,3], Jianjun Zhou[1,3], Wasim Iqbal[1,3], Jixing Ge[1,3], Gleb Fedoseev[1,3], Xia Zhang[1,3], Yanan Feng[1,2], Yong Zhang[1,6,7], Tao Yang[1,8], Xuan Fang[1,6,9], Yihan Wu[1,3], Fangfang Li[1,2,3], Zhenzhen Miao[1,3], Xindi Tang[1,3], Dalei Li[1,3], Yuxin He[1,3], Gang Wu[1,3,10], Weiguang Ji[1,3], and Chuan-Lu Yang[1,11]

[1]*Xinjiang Astronomical Observatory, Chinese Academy of Sciences, Urumqi 830011, China*
[2]*University of Chinese Academy of Sciences, Beijing 100049, China*
[3]*Xinjiang Key Laboratory of Radio Astrophysics, Urumqi 830011, China*
[4]*Key Laboratory of Radio Astronomy and Technology, Chinese Academy of Sciences, Beijing 100101, China*
[5]*Research Center for Astronomical Computing, Zhejiang Laboratory, Hangzhou 311100, China*
[6]*Laboratory for Space Research, Faculty of Science, The University of Hong Kong, Hong Kong, China*
[7]*School of Physics and Astronomy, Sun Yat-sen University, Guangzhou 510275, China*
[8]*State Key Laboratory of Precision Spectroscopy, East China Normal University, Shanghai 200062, China*
[9]*National Astronomical Observatories, Chinese Academy of Sciences, Beijing 100012, China*
[10]*Max-Planck-Institut für Radioastronomie, Auf dem Hügel 69, 53121 Bonn, Germany*
[11]*School of Physics and Optoelectronic Engineering, Ludong University, Yantai 264025, China*

(Received 21 September 2024; accepted manuscript online 22 November 2024)

Sulfur-bearing species are widely utilized to investigate the physical structure of star-forming regions in interstellar media; however, the underlying sulfur chemistry in these environments remains poorly understood. Therefore, further studies of S-bearing species are fundamentally important, as they can enhance our understanding of the physical evolution of star-forming regions. This study presents observations of C_2S and C_3S in L1544, acquired using the Nanshan 26-m radio telescope, along with simulations of their chemical behavior using a one-dimensional physical model. The simulation results reveal significant radial variations in the column densities of C_2S and C_3S. Additionally, the column densities of both molecules are found to be sensitive to the cosmic ray ionization rate at several radial positions, while variations in the C/O ratio have comparatively minimal impact on L1544.

DOI: 10.1088/0256-307X/42/1/019701 CSTR: 32039.14.0256-307X.42.1.019701

1. Introduction. The recent detection of sulfur-bearing carbon chains in TMC-1 and complex organosulfur molecules in the material of comet 67P/Churyumov-Gerasimenko has brought the chemistry of sulfur-bearing species to the forefront of modern astrochemistry. With a cosmic abundance relative to hydrogen (H) of 1.73×10^{-5},[1] sulfur (S) one of the most enigmatic elements in astrochemistry is a vital component of many proteins, alongside more abundant elements, such as hydrogen, carbon (C), oxygen (O), and nitrogen (N).[2] Despite extensive studies of sulfur chemistry in interstellar media (ISM), its complexity, especially in star-forming molecular clouds, remains unresolved. In diffuse ISM regions and photon-dominated regions (PDRs), observed sulfur abundances are close to cosmic values.[3,4] However, in dense molecular clouds, gas-phase sulfur abundance is observed to be only about 0.1% or 1% of the cosmic sulfur abundance,[5] indicating depletion factors as high as three orders of magnitude.[6,7] A major unresolved question is the primary reservoir of sulfur in the ISM. Theoretical models suggest that H_2S could be the most significant sulfur reservoir;[8] however, only OCS and SO_2 have been detected in ice mantles.[9,10]

Pre-stellar core L1544, located in the Taurus molecular cloud at a distance of 170 pc,[11] is characterized by high central densities of approximately 10^6–$10^7\ \mathrm{cm}^{-3}$ and a central temperature of about 6 K.[12,13] This chemically rich core exhibits spatial inhomogeneities in molecular emission distributions.[14,15] Reference [7] examined the sulfur chemistry of L1544, predicting strong radial variations in the abundance of sulfur species. In this study, we present observations of C_2S and C_3S toward L1544 using the Nanshan 26-m radio telescope (NSRT-26 m) at the Xinjiang Astronomical Observatory, complemented by astrochemical modeling to explore sulfur chemistry under varying physical conditions, such as the carbon-to-oxygen (C/O) ratio and cosmic ray ionization rate.

To understand sulfur chemistry in the ISM, it is essential to validate models by observing sulfur-bearing molecules across diverse physical conditions. However, cer-

*Corresponding author. Email: xiaohu.li@xao.ac.cn; donghui.quan@zhejianglab.com

tain conditions, such as the C/O ratio, remain poorly constrained due to observational limitations. Volatile abundances of carbon and oxygen (in both gas and ice phases) often have uncertainties of about a factor of two,[16,17] leading to substantial discrepancies in astrochemical model predictions.[18] Simulations by Ref. [19] showed that the gas-phase abundance of sulfur-bearing species in Taurus Molecular Clouds (TMC-1) is highly sensitive to the C/O ratio. Additionally, cosmic rays (CRs) significantly influence the chemistry and physics of cold, dense star-forming regions.[20] In such environments, CRs act as primary ionizing agents, driving the complex chemistry of molecular ions. CRs also influence the ionization fraction, which regulates the coupling between the gas and interstellar magnetic fields, as well as the heating of the gas.[21] In this study, the cosmic ray ionization rate is denoted by $\zeta_{\rm CR}$. Reference [22] provides an upper limit of approximately $\zeta_{\rm CR} \approx 10^{-16}\,{\rm s}^{-1}$ based on gas temperature measurements in L1544. Model results from Ref. [21] exclude high cosmic-ray ionization rates ($>10^{-16}\,{\rm s}^{-1}$) and estimate the average cosmic-ray ionization rate to be approximately $\zeta_{\rm CR} \approx 3\times10^{-17}\,{\rm s}^{-1}$ in the low-mass prestellar core L1544. These findings suggest that the cosmic-ray ionization rate in molecular clouds or prestellar cores may differ from the standard value of $\zeta_{\rm CR} \approx 1.3\times10^{-17}\,{\rm s}^{-1}$ typically used in astrochemical models.

2. Observations. Single-point observations of the prestellar core L1544 were conducted using the NSRT-26 m telescope at the Xinjiang Astronomical Observatory, Chinese Academy of Sciences (CAS), in April 2021. The J2000 coordinates of the observation are RA = 05h04m16.60s, Dec = $25^\circ10'48.00''$. The $J_{\rm N} = 2_1 - 1_0$ transition of C_2S and the $J = 4-3$ transition of C_3S were observed, with the spectral line parameters listed in Table 1. Parameters for C_2S and C_3S were obtained from the Cologne Database for Molecular Spectroscopy (CDMS* [23]). During the observations, the system temperature was maintained at ∼40 K. The receiver's back end utilized a Digital Filter Bank with 8192 channels and 64 MHz bandwidth, providing a frequency resolution of 7.8125 kHz, a velocity resolution of 104.8 m·s^{-1} at 22.344 GHz and 101.3 m·s^{-1} at 23.122 GHz. The half-power beam widths (HPBW) were $109''$ and $105''$ for C_2S and C_3S respectively. The antenna temperature ($T_{\rm A}^*$) is related to the main beam brightness temperature ($T_{\rm mb}$) via the main beam efficiency (η), i.e. $T_{\rm mb} = T_{\rm A}^*/\eta$; the value of η for NSRT is approximately 0.6. Observations were performed in position-switching mode, with an integration time of three minutes for each on-source and off-source scan. The total integration time for each molecule was 48 minutes, excluding telescope overhead for position switching. The calibration uncertainty (%) of the NSRT-26 m was 14%.[24] Data processing for C_2S and C_3S was performed using CLASS, a component of the GILDAS software suite†.

Table 1. Spectral line parameters of C_2S and C_3S detected in L1544.

Molecule	Transition	ν (MHz)	$S\mu^2$ (Debye^2)	B (MHz)	$E_{\rm u}$ (K)	rms (mK)	$T_{\rm mb}$ (K)	$\int T_{\rm mb}dv$ (K·km·s^{-1})	$V_{\rm LSR}$ (km·s^{-1})	FWHM (km·s^{-1})
C_2S	$J_{\rm N} = 2_1 - 1_0$	22344.0308	16.43636	6477.75	1.60598	19.17	0.562	0.211 (0.030)	7.160 (0.005)	0.353 (0.010)
C_3S	$J = 4-3$	23122.9836	54.88343	2890.38	2.77441	23.29	0.146	0.057 (0.010)	7.117 (0.023)	0.369 (0.050)

Note. $\int T_{\rm mb}dv$ is the integral intensity, $V_{\rm LSR}$ is the local standard of rest radial velocity, and FWHM is the full-width at half-maximum, the values in parentheses are the corresponding derived errors. The parameters of the molecules are taken from the CDMS.[23]

3. Results. For the C_2S and C_3S lines, the Gaussian fitting routine in CLASS was used to derive line parameters, including the main beam brightness temperature ($T_{\rm mb}$), integrated intensity ($W = \int T_{\rm mb}dv$), local standard of rest radial velocity ($V_{\rm LSR}$), and full width at half maximum (FWHM). These results are summarized in Table 1. The observed spectral lines for C_2S and C3S are shown in Fig. 1. The error in $\int T_{\rm mb}dv$ was calculated using $\sigma_w = \sqrt{({\rm cal}\times W)^2 + [{\rm rms}\times\sqrt{2\times{\rm FWHM}\times\Delta V}]^2}$, where cal represents the calibration uncertainty, ΔV is the velocity resolution, and rms is derived from regions free of obvious spectral lines.

Assuming local thermodynamic equilibrium (LTE) conditions and optical thinness of C_2S and C_3S, the column densities of these species were derived using the following equations:[25,26]

$$N_{\rm tot} = \frac{3k}{8\pi^3\nu}\frac{Q(T_{\rm ex})}{S\mu^2}\frac{e^{E_{\rm u}/kT_{\rm ex}}J_\nu(T_{\rm ex})}{J_\nu(T_{\rm ex}) - J_\nu(T_{\rm bg})}\int T_{\rm mb}dv, \tag{1}$$

where k, $S\mu^2$, $E_{\rm u}$, and ν represent the Boltzmann constant, the product of the total torsion-rotational line strength and the square of the electric dipole moment, the upper level energy, and the rest frequency of the line, respectively. $Q(T_{\rm ex})$ denotes the partition function, which was estimated as follows:

$$Q(T_{\rm ex}) = \frac{kT_{\rm ex}}{hB}e^{(hB/3kT_{\rm ex})}, \tag{2}$$

where $T_{\rm ex}$, h, and B are the excitation temperature, Planck's constant, and rigid rotor rotation constant, respectively. $S\mu^2$, B, and $E_{\rm u}$ are obtained from CDMS[23] and are listed in Table 1. $T_{\rm bg}$ (2.73 K) represents the cosmic background temperature. $J_\nu(T)$ is the equivalent Rayleigh-Jeans temperature defined by

$$J_\nu(T) = \Big(\frac{h\nu}{k}\Big)[e^{(h\nu/kT)} - 1]^{-1}. \tag{3}$$

The calculated column densities for C_2S and C_3S are listed in Table 2. The error in the column density ($\sigma_{N_{\rm tot}}$)

*https://cdms.astro.uni-koeln.de/classic/entries/

†http://www.iram.fr/IRAMFR/GILDAS

was calculated using $\sigma_{N_{\rm tot}} = \sigma_W N_{\rm tot}/W$. Reference [27] observed C_2S ($J_N = 2_1 - 1_0$) and C_3S ($J = 4 - 3$) in L1544 with the Nobeyama-45 m telescope, deriving a column density of $1.8 \times 10^{13}\,{\rm cm^{-2}}$ for C_2S and $4.2 \times 10^{12}\,{\rm cm^{-2}}$ for C_3S, assuming excitation temperatures of 5 K and 5.5 K, respectively. Ref. [7] reported lower column densities for both C_2S and C_3S compared to Ref. [27], indicating discrepancies in the derived values. We determined a C_2S column density of $(4.3 \pm 0.6) \times 10^{12}\,{\rm cm^{-2}}$ at an excitation temperature of 4.9 K and a C_3S column density of $(8.7 \pm 1.6) \times 10^{11}\,{\rm cm^{-2}}$ at an excitation temperature of 7.9 K. Observations of the same molecular transitions using different telescopes can yield varying column densities, potentially due to the effect of the telescope's beam dilution factor, which was not accounted for in either our analysis or that of Ref. [27]. Additionally, differences in the calculation methods may contribute to variations in the derived column densities. The previous results for these molecules' column densities are summarized in Table 2. Except for the results from Ref. [27], our findings are generally consistent with other determinations.

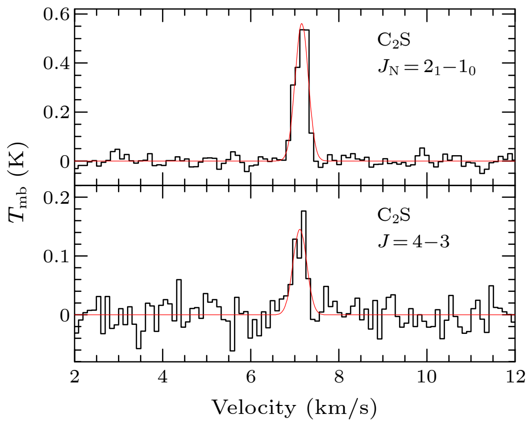

Fig. 1. The detected molecular emissions for C_2S and C_3S in L1544 are illustrated in Fig. 1. The black line represents the observed spectral line profile, and the red line corresponds to the Gaussian fit. The molecule names and rotational transitions are indicated in the upper right corners of the respective panels.

4. Models. The physical model of L1544 is based on a one-dimensional quasi-equilibrium Bonnor–Ebert sphere developed by Ref. [30], which reproduces the observed $C^{18}O$, H_2O, and N_2H^+ lines. The model provides radius-dependent values for H_2 density, gas temperature ($T_{\rm gas}$), dust temperature ($T_{\rm dust}$), and visual extinction ($A_{\rm V}$), as shown in Fig. 2.

In this study, we utilized the Nautilus three-phase model,[31] which accounts for the gas phase, the dust surface (top two layers of ice mantles), and the bulk of the ice mantles. The chemical network was derived from Ref. [32], which extended the sulfur chemical network to explain the observed abundances of sulfur-containing species in TMC-1. Reference [7] demonstrated that significant sulfur depletion is required to reproduce the observations of the prestellar core L1544, leading us to adopt an S/H ratio of 8.0×10^{-8}. Recent studies of dark clouds[32,33] employed a C/O ratio of 0.7 or lower to explain the observed abundances of sulfur-bearing species. We modeled the chemical composition by varying the C/O ratio through adjustments in the C^+ abundance, presenting models with C/O ratios of 0.5, 0.7, and 0.9. The initial conditions are listed in Table 3. For the cosmic ray ionization rate, we tested three scenarios: (1) the standard value commonly used in astrochemical models, $\zeta_{\rm CR} \approx 1.3 \times 10^{-17}\,{\rm s^{-1}}$; (2) an average cosmic ray ionization rate of $\zeta_{\rm CR} \approx 3 \times 10^{-17}\,{\rm s^{-1}}$ for L1544 derived by Ref. [21]; and (3) a high cosmic ray ionization rate of $\zeta_{\rm CR} \approx 1 \times 10^{-16}\,{\rm s^{-1}}$. We simulated the chemical evolution over 10^6 years and compared the results of our chemical modeling with observational data for C_2S and C_3S in L1544. Column densities were calculated using a method adapted from Ref. [7].

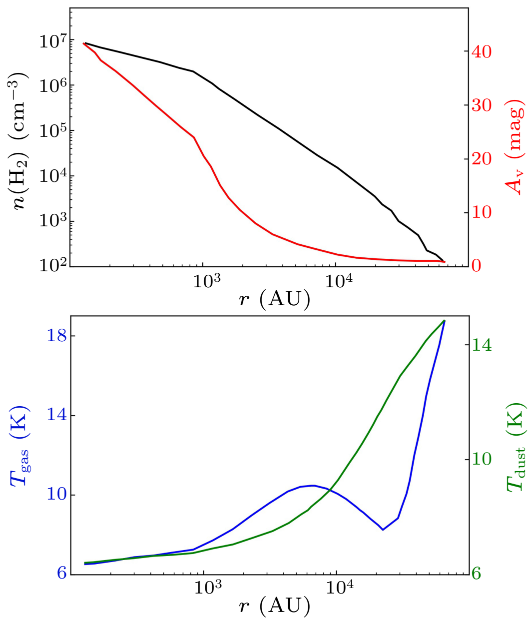

Fig. 2. The employed physical models in this work, extracted from the work of Keto and Caselli (2010). The number density of H_2 [$n(H_2)$, top panel, black line], visual extinction ($A_{\rm V}$, top panel, red line), gas temperature ($T_{\rm gas}$, bottom panel, blue line), and dust temperature ($T_{\rm dust}$, bottom panel, green line) are plotted as a function of radius from the central core towards the edge of the cloud.

Table 2. Column densities of C_2S and C_3S detected in L1544 in this work and from the literature.

Molecule	$T_{\rm ex}$ (K)	N (cm^{-2})	Note
C_2S	$4.9 \pm 0.2^*$	$(4.36 \pm 0.62) \times 10^{12}$	This work
	5	1.8×10^{13}	Ref. [27]
		$(0.96 - 4.4) \times 10^{12}$	Ref. [28]
	4.9 ± 0.2	$(7.5 \pm 1.3) \times 10^{12}$	Ref. [7]
	8.8 ± 0.19	$(4.9 \pm 0.39) \times 10^{12}$	Ref. [29]
C_3S	$7.9 \pm 0.2^*$	$(8.73 \pm 1.56) \times 10^{11}$	This work
	5.5	4.2×10^{12}	Ref. [27]
	7.9 ± 0.2	$(8.8 \pm 0.7) \times 10^{11}$	Ref. [7]
	9.6 ± 0.11	$(1.2 \pm 0.6) \times 10^{12}$	Ref. [29]

* The value of $T_{\rm ex}$ is taken from Ref. [7].

Figures 3 and 4 show the column density profiles of C_2S and C_3S calculated using different models. Four time steps (1.00×10^5, 2.78×10^5, 4.64×10^5, and 1.00×10^6 years) were selected within the range of 10^5–10^6 years, based on the models in Ref. [34] and Ref. [35] models, as these simulations extend beyond 10^5 years to align with observations. The observed column densities of C_2S and C_3S, presented in Fig. 3 and 4, fall within the range summarized in Table 2 (indicated by the gray shaded area), while the black dashed line represents the column density calculated in this study.

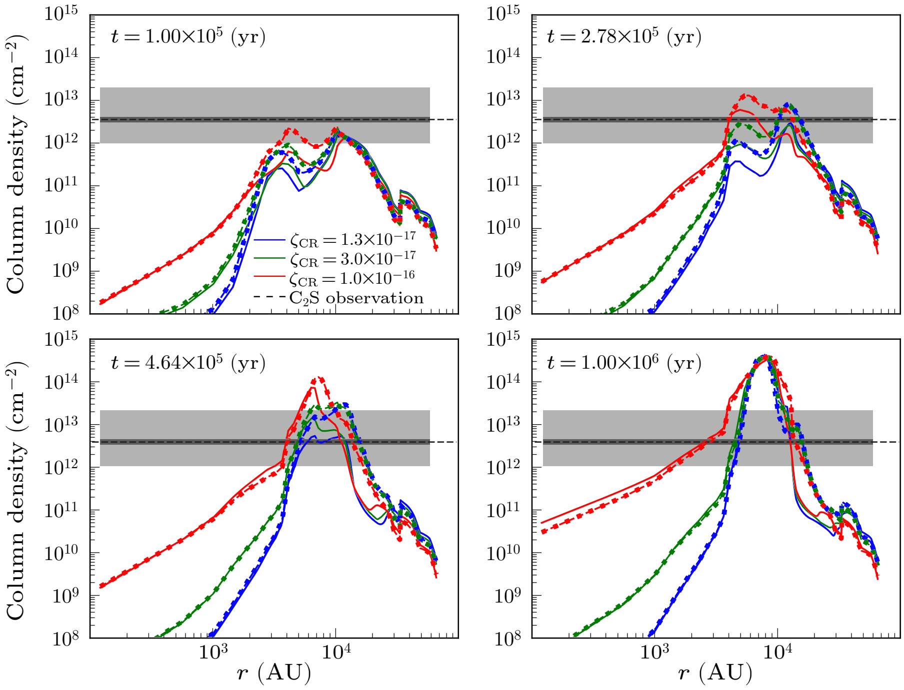

Fig. 3. The column density of C_2S is presented as a function of radius from the central core to the cloud edge at four selected representative evolutionary time points. The results for various models are shown using different colors, with each color representing simulations based on distinct cosmic-ray ionization rate models. The solid line corresponds to C/O = 0.5, the dashed line represents C/O = 0.7, and the dotted line indicates C/O = 1.0. The black dashed line reflects the column density calculated in this study, the black shaded area represents the uncertainty, while the gray shaded area denotes the range of column densities summarized in Table 2.

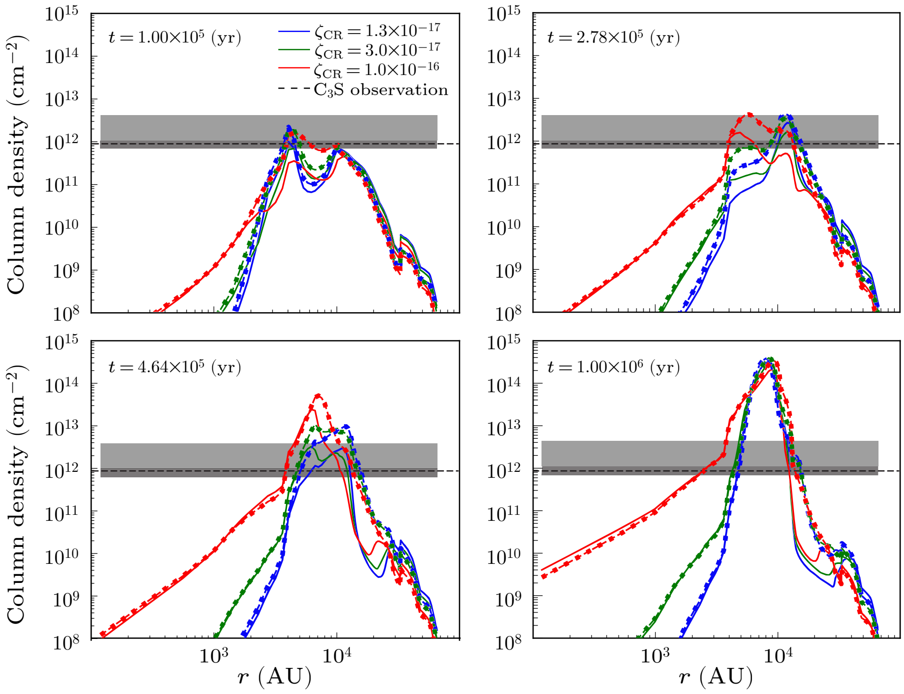

Fig. 4. Same as Fig. 3 but for the molecule of C_3S.

The modeling results demonstrate significant radial variation in the column densities of C_2S and C_3S. For both molecules, column densities peak at distances between 5×10^3 and 10^4 AU across different models at ages exceeding 1×10^5 years. In these models, the primary formation reaction routes for C_2S are as follows:

$$HC_2S^+ + e^- \rightarrow H + C_2S, \tag{4}$$
$$HC_3S^+ + e^- \rightarrow CH + C_2S. \tag{5}$$

Near the 10^4 AU position, C_2S can also be produced by the following reaction:

$$C + HCS \rightarrow C_2S + H. \tag{6}$$

HCS is formed via the reaction of C with H_2S, which itself is produced on dust grains and subsequently released into the gas phase. The main destructive reactions of C_2S occur at distances ranging from 10^3 to 10^5 AU.

$$C_2S + C^+ \rightarrow S + C_3^+, \tag{7}$$
$$C_2S + C^+ \rightarrow C + C_2S^+, \tag{8}$$
$$C_2S + H_3^+ \rightarrow H_2 + HC_2S^+. \tag{9}$$

For C_3S, the main formation reactions at all positions areas follows:

$$HC_3S^+ + e^- \rightarrow H + C_3S, \tag{10}$$

C_3S is mainly destroyed by C^+ at positions ranging from 10^3 to 10^5 AU.

$$C_3S + C^+ \rightarrow S + C_4^+, \tag{11}$$
$$C_3S + C^+ \rightarrow CS + C_3^+, \tag{12}$$
$$C_3S + C^+ \rightarrow C_3 + CS^+. \tag{13}$$

When comparing the simulation results (represented by the red, green, and blue lines) with the observations (indicated by the black dashed horizontal line), we find that at an age of 1×10^5 years, the column density of C_2S matches the observational values at the 10^4 AU position for each model. In contrast, for C_3S, the column density reaches observational values near 5×10^3 AU for some models at the same age of 1×10^5 years. By 2.78×10^5 years, the column densities of both C_2S and C_3S align with observational values at similar positions across different models. At a cloud age of 10^6 years, each model shows a peak column density for C_2S and C_3S at 10^4 AU. These modeling results suggest that C_2S and C_3S likely originate from regions approximately 2×10^3 to 10^4 AU from the central core, corresponding to the external layer of the pre-stellar core.

The column densities of C_2S and C_3S were found to be relatively insensitive to variations within the chosen range of C/O ratios. Notably, only at distances around 10^4 AU do the models with C/O ratios of 0.5 and 0.7 show significant differences, with the column densities calculated for the C/O = 0.7 model being higher than those for the C/O = 0.5 model. Additionally, models with C/O ratios of 0.7 and 1.0 yield nearly identical results for both C_2S and C_3S.

Table 3. The initial elemental abundances used in our models.

Species	n_i/n_H	Reference
H_2	0.5	
He	9.0×10^{-2}	[36]
C^+	1.7×10^{-4}	[37]
N	6.2×10^{-5}	[37]
O	2.4×10^{-4}	[38]
S^+	8.0×10^{-8}	[7]
Si^+	8.0×10^{-8}	[39]
Fe^+	3.0×10^{-9}	[39]
Na^+	2.0×10^{-9}	[39]
Me^+	7.0×10^{-9}	[39]
P^+	2.0×10^{-10}	[39]
Cl^+	1.0×10^{-9}	[39]
F	6.7×10^{-9}	[40]

Furthermore, the cosmic ray ionization rate may influence the column densities of C_2S and C_3S, particularly at ages less than 4.64×10^5 years and a distance of 10^4 AU. A higher cosmic-ray ionization rate results in increased column densities of C_2S and C_3S. CRs are the primary ionizers of gases and influence the chemical properties by generating ions and electrones. The ionization of hydrogen molecules by CRs produces ions,

$$CR + H_2 \rightarrow H_2^+ + e^- + CR, \tag{14}$$

both C_2S and C_3S molecules were produced through the reaction of ions with e^- [Eqs. (4), (5), and (10)]. Therefore, a higher cosmic ray ionization rate leads to an increased column density of these molecules. Recent theoretical models have characterized the increase in CRs decay with increasing density.[21] Given that the column density of H_2 in L1544 decreases radially (Fig. 2), this raises the question of whether CRs levels also vary radially. The column densities of C_2S and C_3S exhibit significant radial variation and are moderately sensitive to changes in the cosmic-ray ionization rate, making them valuable probes for studying CRs. However, the chemical network for sulfur-bearing species remains incomplete. To address this limitation, we plan to use higher spatial resolution observations in conjunction with astrochemical modeling to explore the chemistry of sulfur-containing molecules across diverse interstellar environments.

5. Conclusion. In this work, we present observations of C_2S and C_3S in L1544 using the NSRT-26 m telescope and perform one-dimensional astrochemical modeling of these species to investigate the effects of the C/O ratio and cosmic-ray ionization rate on their formation pathways. Assuming LTE conditions, the calculated column densities for C_2S and C_3S were $(4.4 \pm 0.6) \times 10^{12}$ and $(8.7 \pm 1.6) \times 10^{11}$, respectively. A comparison of the modeled column densities with the observationally derived values indicates that C_2S and C_3S likely originate from the outer layers of the core. We analyzed the impact of the C/O ratio and cosmic-ray ionization rate on the column densities of these molecules. Our findings reveal that while the column densities of C_2S and C_3S are relatively insensitive to variations within the chosen range of C/O ratios in

L1544, they exhibit sensitivity to changes in the cosmic-ray ionization rate at specific locations. Consequently, C_2S and C_3S, alongside other molecular species, could serve as effective probes for measuring cosmic-ray ionization rates.

The characterization of CRs remains an active area of research in astrophysics, with robust constraints on cosmic-ray ionization in astrophysical contexts still being scarce. In recent years, China's Five-hundred-meter Aperture Spherical Radio Telescope (FAST) has achieved significant advancements in various fields of astronomy. L1544, a prototypical prestellar core transitioning from the starless to protostellar phase, has been studied using FAST. Reference [41] reported the detection of magnetic field in L1544 with FAST. According to Ref. [42], the cold HI gas traced by HI narrow line self-absorption (HINSA) within molecular clouds can only be explained by cosmic-ray dissociation. FAST provides a unique opportunity to probe HINSA.[43] Additionally, the FAST Core Array project plans to integrate FAST instruments into synthetic-aperture arrays,[44] which is expected to enhance molecular detection capabilities. Combined observations with FAST and astrochemical modeling will contribute to a deeper understanding of the interactions between CRs and the interstellar medium.

Acknowledgements. X.H.L. acknowledges the support from the Natural Science Foundation of Xinjiang Uygur Autonomous Region (Grant No. 2024D01E37) and the National Science Foundation of China (Grant No. 12473025). This study was funded by the National Natural Science Foundation of China (Grant Nos. 12373026, 12203091, 12173075, and 11973076). WI, JG, and GF would like to thank the Xinjiang Tianchi Talent Program (2024). Tao Yang is grateful for the support from the Xinjiang Tianchi Talent Program (2023) and the Shanghai Natural Science Foundation (Grant No. 22ZR1421400). Xia Zhang thanks the Natural Science Foundation of Xinjiang Uygur Autonomous Region (Grant No. 2022D01A156). It was also partially funded by the Regional Collaborative Innovation Project of Xin jiang Uyghur Autonomous Region (Grant No. 2022E01050). We thank the assistance of the NSRT operators during the observations. The Nanshan 26 m Radio Telescope was partly supported by the Operation, Maintenance, and Upgrading Fund for Astronomical Telescopes and Facility Instruments funded by the Ministry of Finance of China and administered by the Chinese Academy of Sciences.

References

[1] Lodders K 2003 *APJ* **591** 1220

[2] Fontani F, Roueff E, Colzi L, and Caselli P 2023 *A&A* **680** A58

[3] Goicoechea J R, Pety J, Gerin M, Teyssier D, Roueff E, Hily-Blant P, and Baek S 2006 *A&A* **456** 565

[4] Neufeld D A, Godard B, Gerin M, Pineau des Forêts G, Bernier C, Falgarone E, Graf U U, Güsten R, Herbst E, Lesaffre P, Schilke P, Sonnentrucker P, and Wiesemeyer H 2015 *A&A* **577** A49

[5] Tieftrunk A, Pineau des Forets G, Schilke P, and Walmsley C M 1994 *A&A* **289** 579

[6] Wakelam V, Caselli P, Ceccarelli C, Herbst E, and Castets A 2004 *A&A* **422** 159

[7] Vastel C, Quénard D, Le Gal R, Wakelam V, Andrianasolo A, Caselli P, Vidal T, Ceccarelli C, Lefloch B, and Bachiller R 2018 *Monthly Notices of the Royal Astronomical Society* **478** 5514

[8] Bockelée-Morvan D, Lis D C, Wink J E, Despois D, Crovisier J, Bachiller R, Benford D J, Biver N, Colom P, Davies J K, Gérard E, Germain B, Houde M, Mehringer D, Moreno R, Paubert G, Phillips T G, and Rauer H 2000 *A&A* **353** 1101

[9] Palumbo M E, Geballe T R, and Tielens A G G M 1997 *ApJ* **479** 839

[10] Boogert A C A, Schutte W A, Helmich F P, Tielens A G G M, and Wooden D H 1997 *A&A* **317** 929

[11] Galli P A B, Loinard L, Bouy H, Sarro L M, Ortiz-León G N, Dzib S A, Olivares J, Heyer M, Hernandez J, Román-Zúñiga C, Kounkel M, and Covey K 2019 *A&A* **630** A137

[12] Crapsi A, Caselli P, Walmsley M C, and Tafalla M 2007 *A&A* **470** 221

[13] Keto E and Caselli P 2010 *Mon. Not. R. Astron. Soc.* **402** 1625

[14] Spezzano S, Caselli P, Bizzocchi L, Giuliano B M, and Lattanzi V 2017 *A&A* **606** A82

[15] Redaelli E, Bizzocchi L, Caselli P, Sipilä O, Lattanzi V, Giuliano B M, and Spezzano S 2019 *A&A* **629** A15

[16] Jenkins E B 2009 *The Astrophysical Journal* **700** 1299

[17] Whittet D C B 2010 *The Astrophysical Journal* **710** 1009

[18] Bergin E A, Goldsmith P F, Snell R L, and Langer W D 1997 *ApJ* **482** 285

[19] Iqbal W, Li X H, Tuo J, Szczerba R, Feng Y N, Miao Z Z, Yang J C, Ge J X, Fedoseev G, Quan D H, Chang Q, Yang C L, Yang T, Hou G L, Zhang Y, Fang X, Zhang X, Li F F, Ma R, Song X M, Kou Z P, and Sun Y X 2024 *Chin. Phys. Lett.* **41** 029501

[20] Bovino S, Ferrada-Chamorro S, Lupi A, Schleicher D R G, and Caselli P 2020 *MNRAS* **495** L7

[21] Redaelli E, Sipilä O, Padovani M, Caselli P, Galli D, and Ivlev A V 2021 *A&A* **656** A109

[22] Ivlev A V, Silsbee K, Sipilä O, and Caselli P 2019 *The Astrophysical Journal* **884** 176

[23] Müller H S P, Schlöder F, Stutzki J, and Winnewisser G 2005 *Journal of Molecular Structure* **742** 215

[24] Wu G, Qiu K P, Esimbek J, Zheng X W, Henkel C, Li D L, and Han X H 2018 *A&A* **616** A111

[25] Caselli P, Walmsley C M, Zucconi A, Tafalla M, Dore L, and Myers P C 2002 *ApJ* **565** 344

[26] Mangum J G and Shirley Y L 2015 *PASP* **127** 266

[27] Suzuki H, Yamamoto S, Ohishi M, Kaifu N, Ishikawa S I, Hirahara Y, and Takano S 1992 *The Astrophysical Journal* **392** 551

[28] Lai S P and Crutcher R M 2000 *ApJS* **128** 271

[29] Agundez M, Marcelino N, Cernicharo J, Roueff E, and Tafalla M 2019 *A&A* **625** A147

[30] Keto E, Caselli P, and Rawlings J 2015 *MNRAS* **446** 3731

[31] Wakelam V, Ruaud M, Hersant F, Dutrey A, Semenov D, Majumdar L, and Guilloteau S 2016 *A&A* **594** A35

[32] Vidal T H G, Loison J C, Jaziri A Y 2017 *MNRAS* **469** 435

[33] Laas J C and Caselli P 2019 *A&A* **624** A108

[34] Chacón-Tanarro A, Caselli P, Bizzocchi L, Pineda J E, Sipilä O, Vasyunin A, Spezzano S, Punanova A, Giuliano B M, and Lattanzi V 2019 *A&A* **622** A141

[35] Riedel W, Sipilä O, Redaelli E, Caselli P, Vasyunin A I, Dulieu F, and Watanabe N 2023 *A&A* **680** A87

[36] Guilloteau S, Dutrey A, Piétu V, and Boehler Y 2011 *A&A* **529** A105

[37] Piétu V, Dutrey A, and Guilloteau S 2007 *A&A* **467** 163

[38] Hincelin U, Wakelam V, Hersant F, Guilloteau S, Loison J C, Honvault P, and Troe J 2011 *A&A* **530** A61

[39] Pizzo R F, de Bruyn A G, Bernardi G, and Brentjens M A 2011 *A&A* **525** A104

[40] Miettinen O, Smolčić V, Novak M, Aravena M, Karim A, Masters D, Riechers D A, Bussmann R S, McCracken H J, Ilbert O, Bertoldi F, Capak P, Feruglio C, Halliday C, Kartaltepe J S, Navarrete F, Salvato M, Sanders D, Schinnerer E, and Sheth K 2015 *A&A* **577** A29

[41] Ching T C, Li D, Heiles C, Li Z Y, Qian L, Yue Y L, Tang J, and Jiao S H 2022 *Nature* **601** 49

[42] Padovani M, Ivlev A V, Galli D, and Caselli P 2018 *A&A* **614** A111

[43] Liu X C, Wu Y F, Zhang C, Tang N Y, Liu T, Wang K, Li D, Qian L, Qin S L, Esimbek J, Wang J Z, Yuan J H, Xu F W, and Yuan L X 2022 *A&A* **658** A140

[44] Jiang P, Chen R R, Gan H Q, Sun J H, Zhu B Q, Li H, Zhu W W, Wu J W, Chen X L, Zhang H Y, and An T 2024 *Astronomical Techniques and Instruments* **1** 84